A Novel Dual-Membranes WGS Reactor with Palladium Alloy and Polyvinyl Alcohol Membranes for Enhanced Hydrogen Recovery

M. Rahimipanah,[a] M. Baniadam,[b*] S. H. Noie Baghban[c] and M. Mahdavian[d]

[a]Department of Chemical Engineering, Faculty of Engineering, Ferdowsi University of Mashhad, Mashhad, Iran, ma.rahimipanah@alumni.um.ac.ir
[b]Department of Chemical Engineering, Faculty of Engineering, Ferdowsi University of Mashhad, Mashhad, Iran, baniadam@um.ac.ir
[c]Department of Chemical Engineering, Faculty of Engineering, Ferdowsi University of Mashhad, Mashhad, Iran, noie@um.ac.ir
[d]Department of Chemical Engineering, Quchan University of Advanced Technologies Engineering, Quchan, Iran, majid_mahdavian@yahoo.com

Original scientific paper
Received: December 6, 2012
Accepted: May 2, 2013

A novel membrane reactor concept including palladium alloy membrane (selective to H_2) and polyvinyl alcohol membrane (selective to CO_2) is proposed for water gas shift reaction. The mathematical model of the reactor is developed for two reactor schemes, namely plug dual-membrane reactor (PDMR) and CSTR dual-membrane reactor (CDMR) with uni-dimensional and non-isothermal conditions. A comparison between PDMR and palladium alloy membrane reactor (PAMR) showed that PDMR volume becomes 30 % less than PAMR with 20 bar increase in feed pressure. Then the effect of Damkholer number, feed composition, and feed pressure on hydrogen recovery and CO conversion for PDMR and CDMR has been studied. Under the same operating conditions, CO conversion in PDMR is 10 % more than CDMR while its temperature decreases. The new proposed reactor configuration could pave the way for simultaneous production of hydrogen, increased CO conversion, and CO_2 separation on an industrial scale.

Key words:
Dual-membrane reactor, water gas shift reaction, palladium alloy membrane, polyvinyl alcohol membrane

Introduction

Fuel cells, which are regarded as one of the most promising energy conversion approaches, have received increasing attention worldwide.[1] They can operate using different fuels (i.e. methanol, H_2), among them hydrogen is the most common in use.[2] In this regard, hydrogen is considered a clean fuel that has a minimum impact on the environment, nearly eliminating the levels of carbon dioxide and other greenhouse gas emissions, and thus safe, reliable, and –environmentally-friendly energy carrier. One of the most common ways of producing hydrogen is to obtain it from hydrocarbons in processes such as steam reforming (SR), coal gasification (CG), and autothermal reforming (ATR). The H_2 produced from the above reactions contains significant amounts of CO, which is undesirable because it poisons the fuel cell catalyst. A common option for reducing the CO concentration is the water gas shift (WGS) reaction.[2]

$$CO + H_2O \leftrightarrow CO_2 + H_2 \qquad \Delta H^o = -41.4 \text{ kJ mol}^{-1} \qquad (1)$$

In the above equation, ΔH^o is heat of reaction at standard conditions, i.e. 25 °C and 101.325 kPa. This reaction is an equilibrium reaction with a small equilibrium constant. The CO conversion in traditional reactors (TR) without membrane is strongly limited by equilibrium. An attractive alternative to the TR is the Membrane Reactor (MR). In such reactors, a dense membrane (e.g., Pd–Ag supported on a porous substrate) is used to shift the equilibrium by means of selective permeation of one of the reaction products (e.g., H_2).[3]

There are many simulation studies on water gas shift MR.[2–13] Boutikos et al. studied different system parameters, among them being the comparison of CO conversion in different systems with different membrane permeation, the comparison of different catalysts including $Cu/ZnO/Al_2O_3$, Fe_2O_3/Cr_2O_3 and the effect of operating parameters such as inlet temperature and pressure.[2]

Using non-isothermal and steady-state simulation on palladium alloy membrane reactor (PAMR), Piemonte et al. concluded that the increase in PAMR slenderness (ratio of length to diameter) would have a great influence on hydrogen purity.[13]

Huang et al. studied operating parameters impact for polyvinyl alcohol membrane reactor (VAMR), which is a CO_2 selective membrane. By

*Corresponding author: Majid Baniadam Tel.: +98-511-8805031; Fax: +98-511-8816840; E-mail: baniadam@um.ac.ir

adjusting the operating parameters, they enhanced hydrogen recovery to 97 %, and decreased CO at exit to 10 ppm.[7,8]

Here, in order to both increase hydrogen recovery and decrease CO concentration, a novel membrane reactor scheme with two membranes is proposed. The dual-membrane reactor (DMR) is composed of palladium alloy and polyvinyl alcohol membranes which are permeable to H_2 and CO_2 respectively. The developed mathematical model for the reactor is unidimensional, steady, and non-isothermal. The performance of the plug dual-membrane reactor (PDMR) is compared with CSTR dual-membrane reactor (CDMR) under different operating conditions and feed types.

Reactor model

Palladium alloy membrane (H_2-selectivity membrane) and polyvinyl alcohol (CO_2-selectivity membrane) are used in DMR, concurrently. Since the melting point of polymeric membrane is 230 °C, $CuO/ZnO/Al_2O_3$ catalyst is necessary for reaching the reaction. In the DMR, the feed enters the annulus part which has a catalyst bed (Fig. 1); in the same direction sweeping gases enter the shell and tube parts. A mathematical model of the PDMR was developed with the following assumptions:

1. Non-isothermal, unidimensional, and steady-state operation
2. No radial distributions of temperature and concentration in tube or in shell side
3. Negligible axial dispersions of mass and energy
4. Isobaric conditions
5. Infinite hydrogen selectivity of the H_2 selective membrane
6. Co-current flows
7. Ideal gas behavior

$$F_i = \frac{p_i}{RT}\left(Volumetric\ \ flow\ rate\right) \tag{2}$$

For CDMR, only the assumption numbers 4, 5 and 7 were taken into consideration.

Mass balance

Mass balance for PDMR with abovementioned assumptions result in the following equations and boundary conditions:

$$\frac{dF_i^{An}}{dz} = \nu_i r_{co} A^{An\ C-S} - J_i^p A^{pd\,m} - \mu_i^p \Delta p_i A^{VAm} \tag{3}$$

$$B.C.\ F_i^{An}\Big|_{z=0} = F_i^f \tag{4}$$

$$\nu = \begin{cases} +1\ for\ CO_2\ and\ H_2 \\ -1\ for\ CO\ \ and\ H_2O \end{cases}$$

Where Z is reactor length, F_i^{An} is flow rate of each component, $A^{pd\,m}$ is H_2 selective membrane surface area, and $A^{An\ C-S}$ is cross section area of annulus side.

Also, mass balance equations in tube and shell part can be written as:

$$\frac{dF_i^{Sh}}{dz} = J_i^p A^{pd\,m} \tag{5}$$

$$B.C.\ F_i^{Sh}\Big|_{z=0} = F_i^S \tag{6}$$

$$\frac{dF_i^{Tu}}{dz} = \mu_i^p \Delta p_i A^{VAm} \tag{7}$$

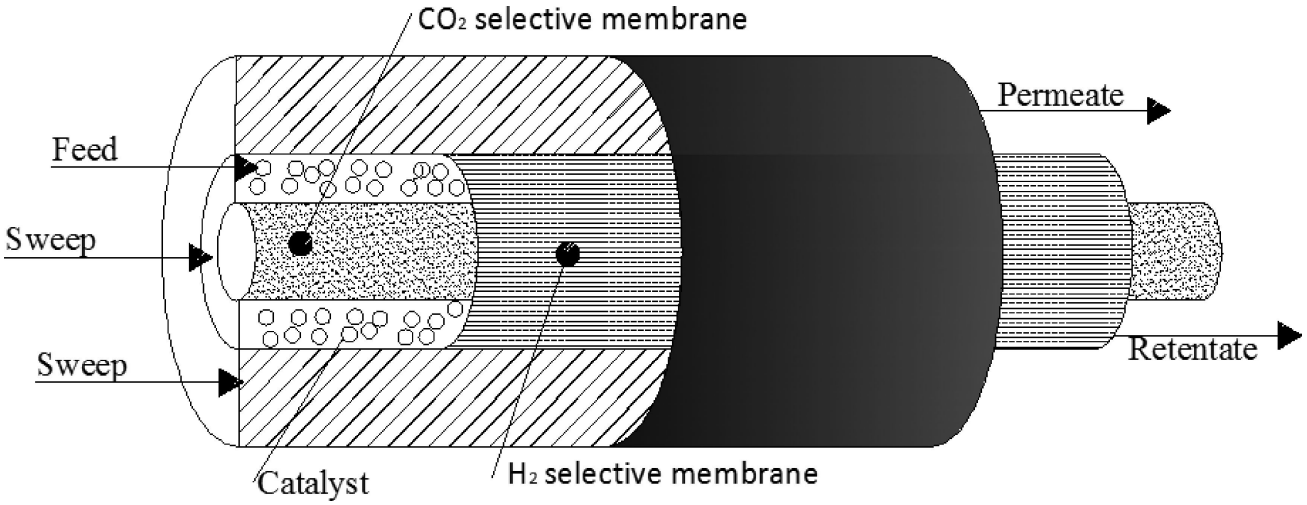

Fig. 1 – *Representation of the proposed DMR scheme*

$$B.C.\ F_i^{Tu}\Big|_{z=0} = F_i^S \tag{8}$$

In equations (3) and (5) J_i^p is flux of hydrogen and is described by the Sieverts' law:[6]

$$J_i^p = \begin{cases} 46.4e^{-4}\exp(-\frac{644}{RT})(p_{H_2}^{An\,0.552} - p_{H_2}^{Sh\,0.552}) & for\ i=H_2 \\ 0 & for\ i\neq H_2 \end{cases} \tag{9}$$

The last term of equations 3 and 7 shows polyvinyl alcohol membrane permeation. The properties of the CO_2 selective membrane for the simulations are listed in Table 1. It should be noted that while the dual-membrane reactor was considered previously for methanol production,[14,15] practical use of such reactors for hydrogen production involves construction issues, which must be considered in detail. Reaction rate r_{co} is presented through kinetics equations introduced by Ayastuy et al.:[16]

Table 1 – *Reference membrane*

Material/name	Pebax/PG
Permeability- CO_2	$(9.41\times10^{-8})10^{-10}$ kmol s^{-1} bar^{-1} m^{-1}
Selectivity CO_2/H_2	15.5
Selectivity	47
Selectivity	47

$$-r_{co} = \frac{k(p_{CO}p_{H_2O} - \frac{p_{CO_2}p_{H_2}}{K_e})}{(1+K_{CO}p_{CO}+K_{H_2O}p_{H_2O}+K_{H_2}^{0.5}p_{H_2}^{0.5}+K_{CO_2}p_{CO_2}p_{H_2}^{0.5})^2}\times\frac{1}{3.6} \tag{10}$$

The mass balances equations, as well as their initial conditions (I.C.) for each species in CDMR are given by equations (11) to (16), respectively:

$$\frac{1}{RT^{An}}\frac{dp_i^{An}}{dt} = \frac{F_i^{An}-F_i^F}{V^{An}} + \nu_i r_{co} - \frac{A^{Pd\,m}}{V^{An}}J_i^p - \mu_i^p\Delta p_i\frac{A^{VAm}}{V^{An}} \tag{11}$$

$$I.C.\ p_i^{An} = p_i^{An,I} \tag{12}$$

$$\frac{1}{RT^{Sh}}\frac{dp_i^{Sh}}{dt} = \frac{F_i^{Sh}-F_i^S}{V^{Sh}} + \frac{A^{Pd\,m}}{V^{Sh}}J_i^p \tag{13}$$

$$I.C.\ p_i^{Sh} = p_i^{Sh,I} \tag{14}$$

$$\frac{1}{RT^{Tu}}\frac{dp_i^{Tu}}{dt} = \frac{F_i^{Tu}-F_i^S}{V^{Tu}} + \mu_i^p\Delta p_i\frac{A^{VAm}}{V^{Tu}} \tag{15}$$

$$I.C.\ p_i^{Tu} = p_i^{Tu,I} \tag{16}$$

Energy balance

All the energy balance equations will contain the terms of equations 17 to 19. In the following sections, the energy balances will be written for the PDMR and CDMR treated in the previous section.

$$\Delta T_\Phi = J_{H_2}^p(h_{H_2}^{T^{An}} - h_{H_2}^{T^{Sh}})\ on\ shell\ side \tag{17}$$

$$\Delta T_Y = \mu_i^p\Delta p_i(h_{CO_2}^{T^{An}} - h_{CO_2}^{T^{Tu}})\ on\ tube\ side \tag{18}$$

$$\Psi = r_{CO}(-\Delta H_r) \tag{19}$$

Where ΔT_Φ is the temperature variation due to enthalpy flux associated with hydrogen permeation, ΔT_Y is the temperature variation due to enthalpy flux associated with CO_2 permeation, and Ψ is the heat produced by chemical reaction.

Equations (20) to (25) give the energy balance for annulus, shell, and tube sides in PDMR, respectively, when the reaction takes place in the annulus:

$$\frac{dT^{An}}{dz} = \left(\frac{1}{\sum_{i=1}^{n}F_i c_{p_i}}\right)\cdot \left(\Psi A^{An\,C-S} - U_{A-T}A^{VAm}(T^{An}-T^{Tu}) - U_{A-S}A^{Pd\,m}(T^{An}-T^{Sh}) - \Delta T_\Phi A^{Pd\,m} - YA^{VAm}\right) \tag{20}$$

$n = number\ of\ species\ in\ annulus\ side$

$$B.C.\ T^{An}\Big|_{z=0} = T^F \tag{21}$$

$$\frac{dT^{Sh}}{dz} = \left(\frac{1}{\sum_{i=1}^{m}F_i c_{p_i}}\right)\cdot \left(U_{A-S}A^{Pd\,m}(T^{An}-T^{Sh}) + \Delta T_\Phi A^{Pd\,m}\right) \tag{22}$$

$m = number\ of\ species\ in\ shell\ side$

$$B.C.\ T^{Sh}\Big|_{z=0} = T^S \tag{23}$$

$$\frac{dT^{Tu}}{dz} = \left(\frac{1}{\sum_{i=1}^{k}F_i c_{p_i}}\right)\cdot \left(U_{A-T}A^{VAm}(T^{An}-T^{Tu}) + \Delta T_Y A^{VAm}\right) \tag{24}$$

$k = number\ of\ species\ in\ tube\ side$

$$B.C.\ T^{Tu}\Big|_{z=0} = T^S \tag{25}$$

Where T^{An} is annulus side temperature, T^{Sh} is shell side temperature, T^{Tu} is tube side temperature, c_{p_i} special heat of each component, U_{A-T} is the overall heat transfer coefficient between the annulus side and the tube side, and U_{A-S} is the overall heat transfer coefficient between annulus side and shell side.

Energy balance for CDMR is as follows:

$$\sum_{i=1}^{n} C_i c_{p_i} \frac{dT^{An,E}}{dt} = \frac{\left(\sum_{i=1}^{n} F_i c_{p_i} T^{An,E} - \sum_{i=1}^{n} F_i c_{p_i} T^{An,In}\right)}{V^{An}} + \\ + \Psi - \Delta T_{\Phi} \frac{A^{Pdm}}{V^{An}} - \Delta T_{Y} \frac{A^{VAm}}{V^{An}} - \\ - \frac{U_{A-S} A^{Pdm}}{V^{An}} (T^{An,E} - T^{Sh,E}) - \\ - \frac{U_{A-T} A^{VAm}}{V^{An}} (T^{An,E} - T^{Tu,E}) \quad (26)$$

$$n = number\ of\ species\ in\ annulus\ side$$

$$I.C.\ T^{An}\Big|_{t=0} = T^{An,I} \quad (27)$$

$$\sum_{i=1}^{m} C_i c_{p_i} \frac{dT^{Sh,E}}{dt} = \frac{\left(\sum_{i=1}^{m} F_i c_{p_i} T^{Sh,E} - \sum_{i=1}^{m} F_i c_{p_i} T^{Sh,In}\right)}{V^{An}} + \\ + \Delta T_{\Phi} \frac{A^{Pdm}}{V^{Sh}} + \frac{U_{A-S} A^{Pdm}}{V^{Sh}} (T^{An,E} - T^{Sh,E}) \quad (28)$$

$$m = number\ of\ species\ in\ shell\ side$$

$$I.C.\ T^{Sh}\Big|_{t=0} = T^{Sh,I} \quad (29)$$

$$\sum_{i=1}^{n} C_i c_{p_i} \frac{dT^{Tu,E}}{dt} = \frac{\left(\sum_{i=1}^{k} F_i c_{p_i} T^{Tu,E} - \sum_{i=1}^{k} F_i c_{p_i} T^{Tu,In}\right)}{V^{Tu}} + \\ + \Delta T_{Y} \frac{A^{VAm}}{V^{Tu}} + \frac{U_{A-T} A^{VAm}}{V^{Tu}} (T^{An,E} - T^{Tu,E}) \quad (30)$$

$$k = number\ of\ species\ in\ tube\ side$$

$$I.C.\ T^{Tu}\Big|_{t=0} = T^{Tu,I} \quad (31)$$

The performance of the DMR is evaluated by the following three parameters:

– Hydrogen Recovery

$$R_{H2} = \frac{F_{H2}^{p}}{F_{H2}^{p} + F_{H2}^{r}} \quad (32)$$

– Overall CO Conversion

$$X_{CO} = \frac{F_{CO}^{f} - \left(F_{CO}^{p} + F_{CO}^{r}\right)}{F_{CO}^{f}} \quad (33)$$

– Damkohler Number (Da)

$$Da = r_{in}\, m_c / F_{co}^{f} \quad (34)$$

Damkholer number is calculated at reactor entrance. This dimensionless number is the ratio of the mass consumption (or production) due to reaction to the axial transport via convection.[2]

Reactor geometric characteristics, as well as the investigated operating parameters, are presented in Table 2. Feed gas compositions used in the simulations are shown in Table 3. For investigation of the thermal effect in DMR, composition of feed gas is similar to that in ATR process.

Table 2 – *Specifications of simulated DMR and its operating parameters*

Value	Parameter
40 cm	D^{Sh}
30 cm	D^{An}
15 cm	D^{Tu}
100 cm	L
5 bar	p_{in}
1bar	$p_{in,sweep}$
150 °C	T_{in}
130 °C	$T_{in}, sweep$

Table 3 – *Composition feed gases supplied from different processes*

	CG	ATR	SR
CO	0.3790	0.1785	0.0500
CO_2	0.0105	0.0099	0.1152
H_2	0.1883	0.3593	0.6106
H_2O	0.3846	0.4167	0.2222
N_2	0.0304	0.0356	0.0020
S/C	1.014	2.35	4.44

Results and discussion

Since a novel configuration for the membrane reactor is proposed here, there are no operating data for validation. However, we validate the single membrane as the base case and then simulate the novel proposed reactors. Fig. 2 shows the comparison of data obtained from this model and data from Piemonte's work.13

At first, a comparison was made between the performance of DMR and PAMR. To compare the performance of PAMR and TR, the volume index (VI) [11] is used. The VI is an indicator of the modularity of PAMR and it compares the PAMR reaction volume necessary to achieve a set conversion with that of a TR. Analogously, VI is defined as an indi-

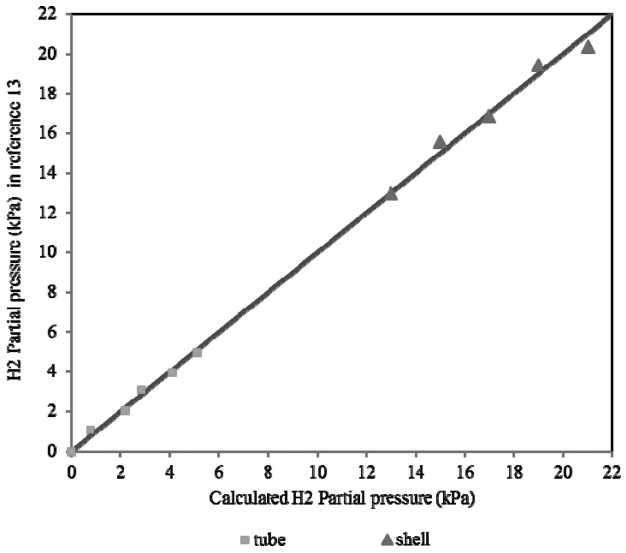

Fig. 2 – *Validation of partial pressure of H2 obtained from the presented model*[13]

cator of the modularity of PDMR and it compares the PDMR reaction volume necessary to achieve a set conversion with that of a PAMR reaction volume:

$$VI = \left. \frac{V_{\text{Reaction side}}^{DMR}}{V_{\text{Reaction side}}^{PMR}} \right|_{\text{set co conversion}} \tag{35}$$

Fig. 3 shows VI versus feed pressures where the temperature is 150 °C and conversion of CO set to 0.9. VI is a decreasing function of the feed pressure for the WGS reaction. This may be attributed to the permeation of hydrogen and carbon dioxide in PDMR, which in turn cause the equilibrium to shift to the right, and a higher conversion than PAMR. Thus, for a given conversion set, PDMR would have a smaller size. With an increase in feed pressure to 20 bar, PDMR volume becomes 30 % less than PAMR.

So far, only Bruneti et al. have studied the effect of hydrogen concentration in feed on the hydrogen recovery and CO conversion. However, feed of WGS reactor is supplied by units like ATR, CG,

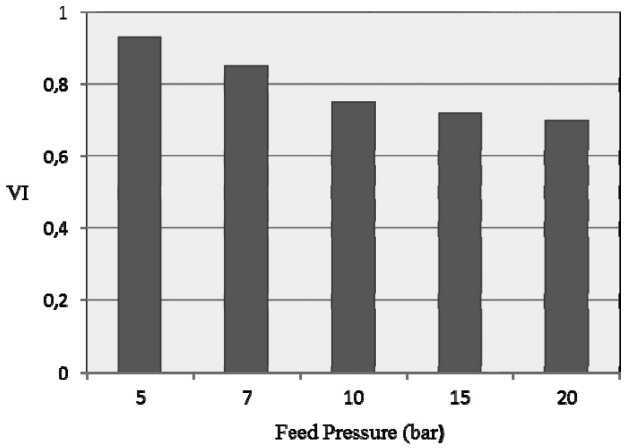

Fig. 3 – *Volume index as a function of feed pressure for the ATR feed. T = 150 °C and CO conversion set = 90 %*

POX and SR with considerably different hydrogen concentration. Therefore, it seems necessary to study the effect of hydrogen concentration of the feed on the performance of WGS reactor. To study the effect of hydrogen content, two types of feed with the same S/C and different hydrogen concentrations are compared. Table 4 shows the complete specifications of the feeds.

Figs. 4 a and b, respectively, show CO conversion and Hydrogen recovery in different Damkholer numbers and different S/Cs for a feed with low hydrogen concentration (FLHC) in a PDMR. Similarly, Figs. 5 a and b, respectively, show CO conversion and Hydrogen recovery in different Damkholer numbers and different S/Cs to feed with high hydrogen concentration (FHHC) in a PDMR.

As can been seen in Figs. 4 and 5, with increasing S/C in a constant Damkholer, hydrogen recovery increases while CO conversion decreases. With increasing S/C in feed, most of the CO is consumed, and production of hydrogen and consequently its recovery reduces.

When FLHC enters the reactor (Fig. 4), optimal Da is between 0.8 to 1. In Fig. 4 b, a sudden increase in hydrogen recovery is observed for Da = 0.8. However, this increase is less for CO conversion. The situation is vice versa for FHHC. In this

Table 4 – *Feed composition*

	Feeds with low hydrogen concentration (FLHC)				Feeds with high hydrogen concentration (FHHC)			
CO	0.475	0.309	0.225	0.175	0.25	0.197	0.125	0.1
CO_2	0	0	0	0	0.1	0.1	0.1	0.1
H_2	0.05	0.05	0.05	0.05	0.4	0.4	0.4	0.4
H_2O	0.475	0.641	0.725	0.775	0.25	0.333	0.375	0.4
S/C	1	2	3	4	1	2	3	4

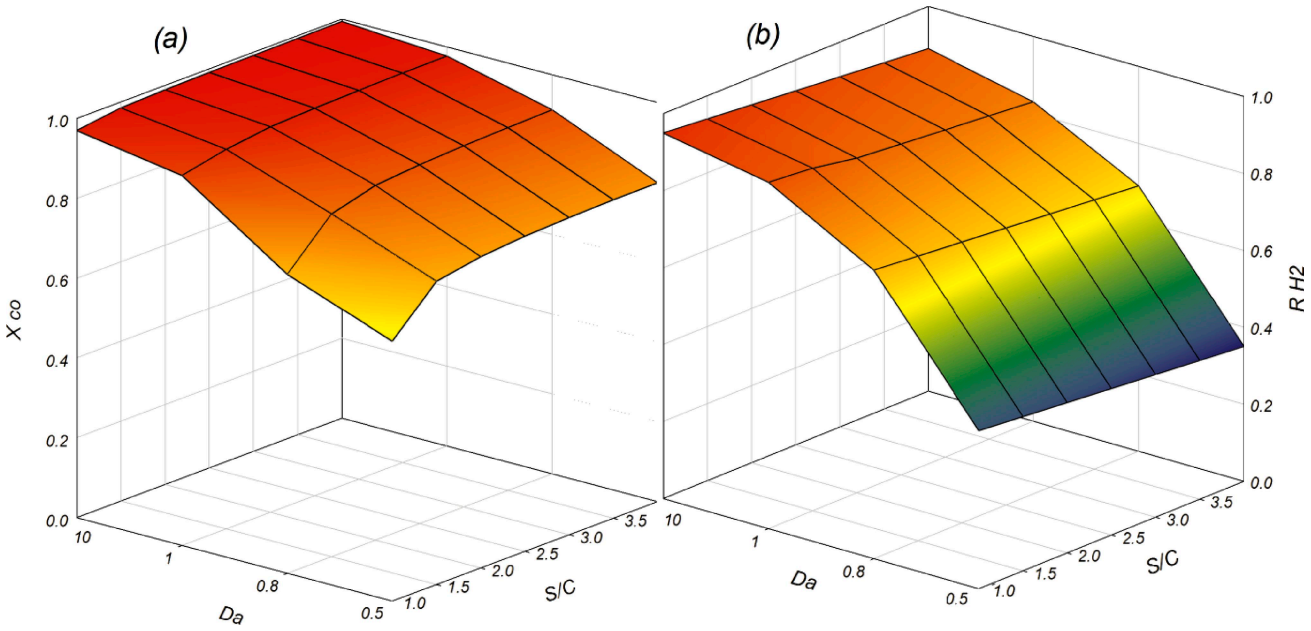

Fig. 4 – *(a) Hydrogen recovery and (b) CO conversion versus Damkholer number and S/C, for FLHC; PDMR*

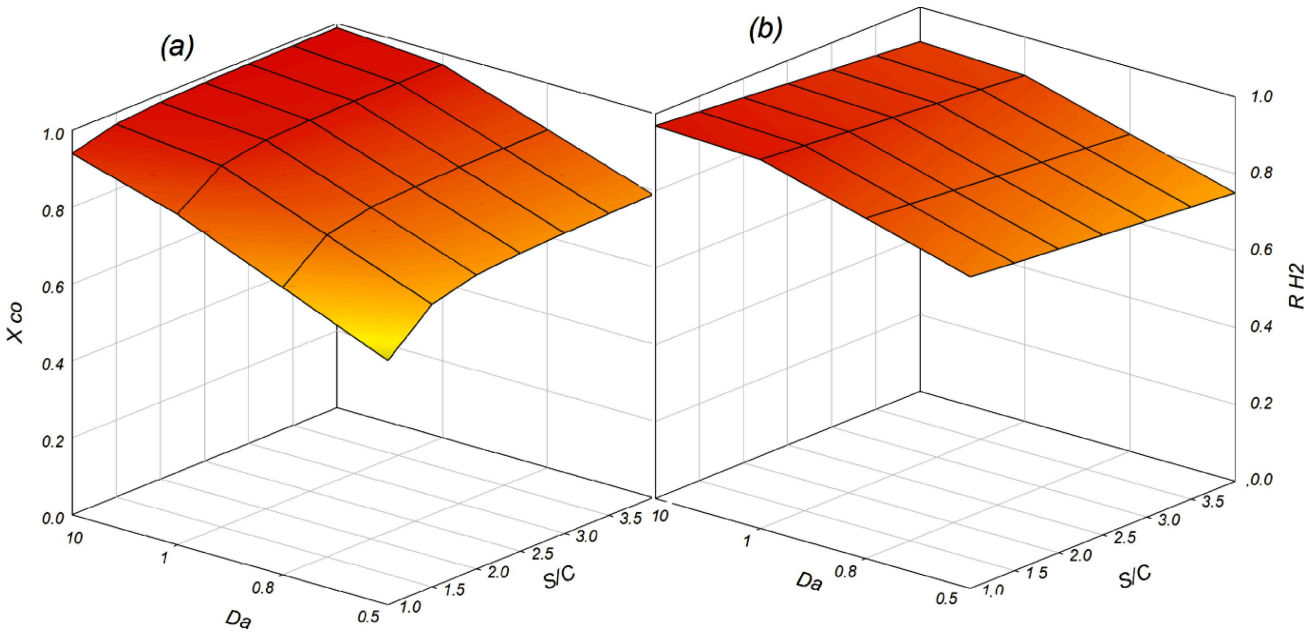

Fig. 5 – (a) Hydrogen recovery and (b) CO conversion versus Damkholer number and S/C, for FHHC; PDMR

feed, high content of H_2 reduces the residence time of the reactants. Thus, in order to reach the desirable increase in residence time, an optimal Da can be identified to be higher than 1.

In low Da, hydrogen recovery for FHHC is considerably higher than FLHC. However, for high Da this difference is lower. In low Da, there is not enough time for hydrogen production and therefore (as it happens for FLHC) there will not be sufficient gradient for transfer of hydrogen from reaction zone. The existence of less hydrogen in reaction side caused a decrease in hydrogen partial pressure gradient, hydrogen permeation, and its recovery. However, in FHHC the gradient will be high from the beginning of the reactor. With increasing Da, the reaction can be completed since the reactants have sufficient time to complete the reaction, and both the production and recovery of hydrogen will increase. For Da>>1 the difference between recovery of FHHC and FLHC significantly decreases.

Comparing Figs. 4 a and 5 a, one can see that CO conversion for FLHC is less than FHHC. For FHHC, residence time is low and CO conversion decreases.

Generally, in Figs. 5 to 8, for Da between 1 to 10, there will be no obvious increase for both hy-

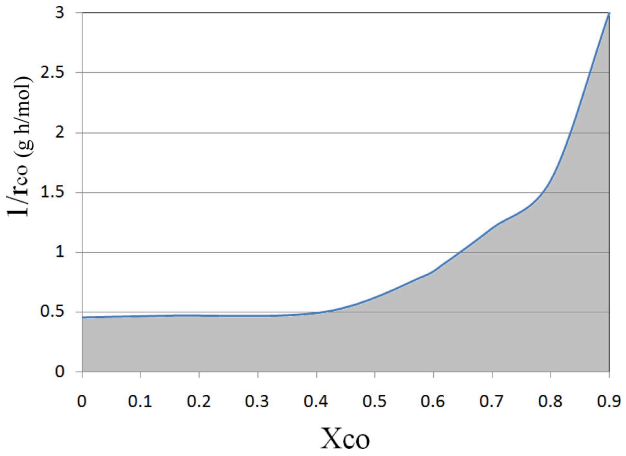

Fig. 6 – *Inverted reaction rate versus CO partial pressure for PDMR*

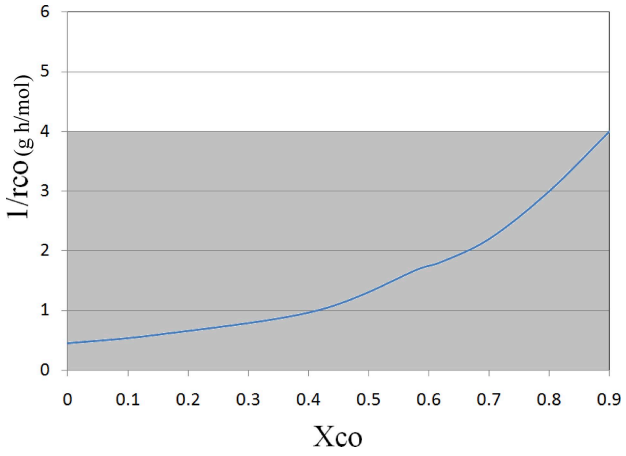

Fig. 7 – *Inverted reaction rate versus CO partial pressure for CDMR*

drogen recovery and CO conversion, therefore, higher Da is not suggested.

In Figs. 6–9, CDMR and PDMR were compared. Residence time for all reactors equaled one second. The travelled distance, rather than time was used in CDMR.

Figs. 6–7 show inverse reaction rate vs. CO conversion for PDMR and CDMR. In these figures, the highlighted area equals space time.[17] For both reactors, the final CO conversion is 0.9. The highlighted area for PDMR is less than CDMR.

In constant CO conversion, CDMR volume is higher than PDMR volume or in equal volumes, PDMR performance is higher. More uniform concentrations prevail inside the CDMR as well as in its effluent stream, and subsequently it applies smaller gradient for transfer of products.

Figs. 8 a and b, show hydrogen recovery versus times for different pressure feeds in PDMR and CDMR.

At pressure less than 10 bar, hydrogen recovery for PDMR has a steep slope; in other words, hydrogen recovery could be enhanced by 0.1 when the pressure is increased from 5 to 10. However, at high pressures, hydrogen recovery is increased by 0.01 for the same increases in pressure (15 to 20 bar).

Since the difference between stoichiometric coefficient equals zero ($\Delta v_i = 0$) for WGS reaction, the pressure difference merely affects the hydrogen permeation. However, P = 10 bar is enough to recover 97 % of hydrogen, and further increase in the pressure has no considerable effect on the enhancement of hydrogen recovery.

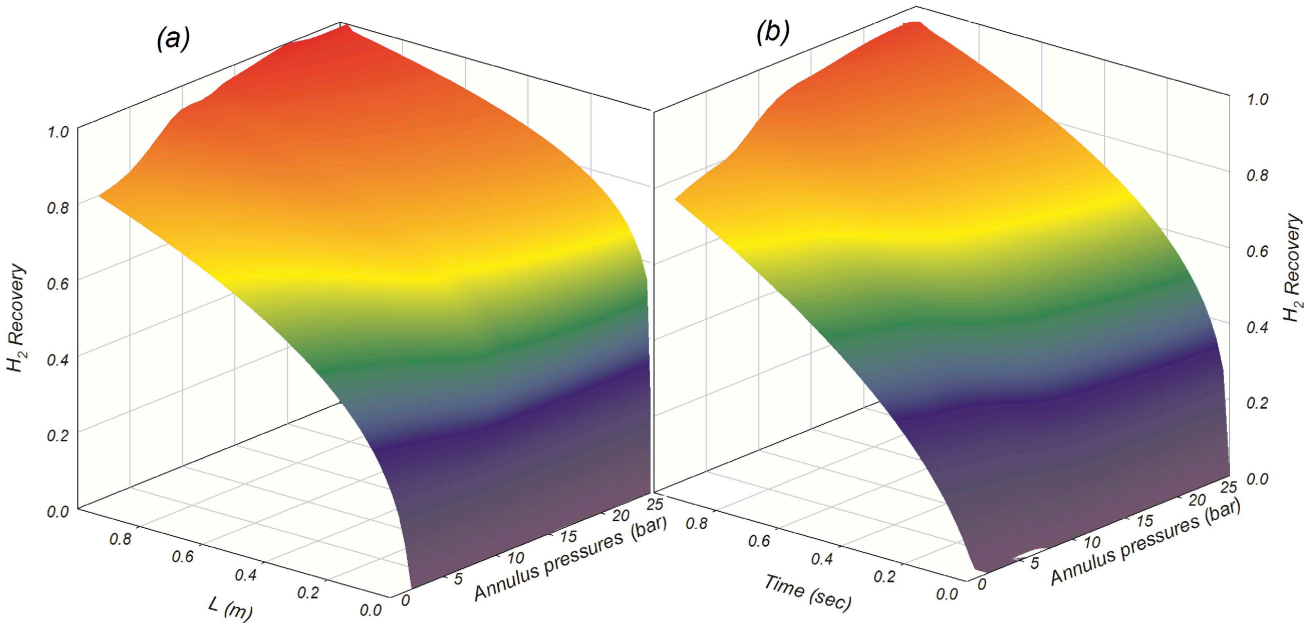

Fig. 8 – Hydrogen recovery versus length and pressure. ATR feed type; T = 150 ˚C; (a) PDMR and (b) CDMR

In PDMR, hydrogen recovery of 0.97 is achieved at lower pressures. According to Figs. 6 and 7, reaction progress in PDMR is more than CDMR, so more hydrogen is produced. The existence of more hydrogen in reaction side caused an increase in hydrogen partial pressure gradient, hydrogen permeation, and recovery.

In Fig. 8 a and b, hydrogen recovery increased with a steep slope at the beginning of reactors, and then with a slight slope at the end. As the reactants move forward in the reactor, they are consumed and their reaction rates decrease. At the same time, the co-current stream of scrubbing gases is enriched with the products. These two factors decrease hydrogen recovery and CO conversion.

Fig. 9 shows temperature distribution in three different regions of DMRs. For a better comparison, the temperature distribution of each region is shown separately and in each figure, two types of DMRs are compared with each other.

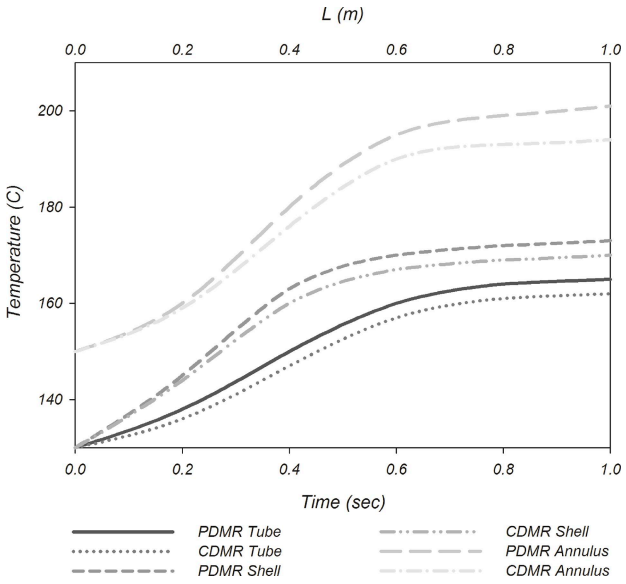

Fig. 9 – *Temperature distribution for PDMR and CDMR*

Melting temperature of CO_2 selective polymeric membrane is close to 230 °C. However, the WGS reaction is exothermic and the temperature of the reaction side must be kept at 210 °C at most.[7]

Two factors can be employed to control the temperature of the system. The first is the temperature of the sweeping gas and feed. Here, the temperatures of feed and sweeping gas are kept at 150 °C and 130 °C, respectively. The other factor used to control the temperature of the reaction zone is S/C. Since water has high specific heat, an increase in steam pressure prevents the temperature from increasing abruptly. Here, high pressure and proper catalyst for low temperatures were applied to compensate the low temperature effect.[14]

Temperature behavior in all three areas is the same, having the same order of magnitude of heat transfer coefficient. However, the shell side with an inorganic membrane exchanges more heat with the reaction zone. Therefore, its temperature becomes higher than that of the tube. Figs. 6 and 7 show that the reaction progresses better in PDMR, so heat production in this type of DMR is higher than in CDMR.

According to Fig. 8, it can be seen that in the same pressures, PDMR hydrogen recovery is higher than with CDMR. This causes a temperature rise in the tube and shell sides for PDMR when compared to the other reactor.

Conclusion

In this study, a novel DMR including both polyvinyl alcohol membrane (selective to CO_2) and palladium alloy membrane (Selective to H_2) was mathematically modeled and simulated for PDMR and CDMR. A comparison was made between PDMR and PAMR, which showed PDMR volume becomes 30 % less than PAMR at high pressure, while CO conversion for PDMR in S/C = 4 is about 10 % more than CDMR. It should be noted that in this DMR, temperature increase is higher than in the other one. When FLHC enters the reactor, optimal Da is between 0.8 to 1. The situation is vice versa for FHHC, in this feed an optimal Da can be identified to be higher than 1. Generally, when reactor was fed with low hydrogen and high steam, WGS reactor performance was higher. The proposed membrane reactor configuration for WGS could both enhance hydrogen recovery and reduce CO_2 emissions.

Appendix A. Kinetic model data

Values of the parameters present in the r_{CO} expression:

$$K_{eq} = \exp(4577.8/T - 4.33) \quad \text{(A-1)}$$

$$k = 2.391\times10^{7}\exp(-6049.2/T) \quad \text{(A-2)}$$

$$K_{CO} = 0.0942\exp(1782.1/T) \quad \text{(A-3)}$$

$$K_{H_2O} = 0.0333\exp(2088.8/T) \quad \text{(A-4)}$$

$$K_{H_2} = 0.0315\exp(2057.7/T) \quad \text{(A-5)}$$

$$K_{CO_2} = 0.00314\exp(3003.5/T) \quad \text{(A-6)}$$

Nomenclature

A^{AnC-S} – Annulus cross section area, m^2
A^{Pdm} – Pd membrane area, m^2
A^{VAm} – VA membrane area, m^2
C_i – i-th component Concentration, mol m^{-3}
c_{p_i} – Heat capacity of component i, kJ mol^{-1} K^{-1}
Da – Damkholer number, –
F_i^{An} – i-th component molar flow rate in annulus side, mol s^{-1}
F_i^{Sh} – i-th component molar flow rate in shell side, mol s^{-1}
F_i^{Tu} – i-th component molar flow rate in tube side, mol s^{-1}
F_i^{f} – i-th component molar flow rate in feed, mol s^{-1}
F_i^{S} – i-th component molar flow rate in sweep gas, mol s^{-1}
h_{H_2} – Hydrogen enthalpy, kJ mol^{-1}
J_i^{P} – Hydrogen flux permeating through the membrane, mol m^{-2} s^{-1}
k – Kinetic constant of the WGS reaction equations (10), mol kg^{-1} s^{-1}
K_e – Equilibrium constant for the WGS reaction equations (10), –
K_i – i-th component adsorption constant, bar^{-1}
m_c – Catalyst mass, g
p_i^{An} – i-th component partial pressure in the annulus side, bar
p_i^{Sh} – i-th component partial pressure in the shell side, bar
p_i^{Tu} – i-th component partial pressure in the tube side, bar
$p_i^{An,I}$ – i-th component partial pressure in the initial time for the annulus side, bar
$p_i^{Sh,I}$ – i-th component partial pressure in the initial time for the shell side, bar
$p_i^{Tu,I}$ – i-th component partial pressure in the initial time for the tube side, bar
μ_i^{p} – Permeability of species i, kmol s^{-1} bar^{-1} m^{-2}
R – Universal gas constant, kJ mol^{-1} K^{-1}
R_{H_2} – Hydrogen recovery, –
r_{CO} – Kinetic rate of WGS reaction, mol kg^{-1} s^{-1}
t – Time, s
T^{An} – Annulus temperature, °C
T^{Sh} – Shell temperature, °C
T^{Tu} – Tube temperature, °C
T^{f} – Feed temperature, °C
T^{Sh} – Sweep gas temperature, °C
$T^{An,I}$ – Annulus temperature at the initial time, °C
$T^{Sh,I}$ – Shell temperature at the initial time, °C
$T^{Tu,I}$ – Tube temperature at the initial time, °C
$T^{An,E}$ – Exit annulus temperature, °C
$T^{Sh,E}$ – Exit shell temperature, °C
$T^{Tu,E}$ – Exit tube temperature, °C
$T^{An,In}$ – Inlet annulus temperature, °C
$T^{Sh,In}$ – Inlet shell temperature, °C
$T^{Tu,In}$ – Inlet tube temperature, °C
U_{A-S} – Overall heat transfer coefficient between annulus side and shell side, kJ m^{-2} s^{-1} °C^{-1}
U_{A-T} – Overall heat transfer coefficient between annulus side and shell side, kJ m^{-2} s^{-1} °C^{-1}
V^{An} – Annulus volume, m^3
V^{Sh} – Shell volume, m^3
V^{Tu} – Tube volume, m^3
X_{CO} – conversion, –
z – Axial coordinate, m

Greek letters

ΔH_r – Reaction enthalpy, kJ mol^{-1}
ν_i – Stoichiometric coefficient with respect to the reference component of ith species, –

Superscripts and subscripts

An – Annulus
E – Equilibrium
E – Exit
F – Feed
I – Initial
i – i-th component
In – Inlet
P – Permeate
Pd m – Pd alloy membrane
R – Retentate
S – Sweep
Sh – Shell
Tu – Tube
VA m – Vinyl alcohol membrane

Reference

1. *Zou, J., Huang, J., Ho, W. S. W.,* Ind. Eng. Chem. Res. **46** (2007) 2272.
2. *Boutikos, P., Nikolakis, V.,* J. Membr. Sci. **350** (2010) 378.
3. *Adrover, M. E., Anzola, A., Schbib, S., Pedernera, M., Borio D.,* Catal. Today **156** (2010) 223.
4. *Adrover, M. E., López, E., Borio, D. O., Pedernera, M. N.,* Chem. Eng. J. **154** (2009) 196.
5. *Gosiewski, K., Tanczyk, M.,* Catal. Today **176** (2011) 373.
6. *Gosiewski, K., Warmuzinski, K., Tanczyk, M.,* Catal. Today **156** (2010) 229.
7. *Huang, J., El-Azzami, L., Ho, W. S. W.,* J. Membr. Sci. **261** (2005) 67.
8. *Huang, J., Ho, W. S. W.,* J. Chin. Inst. Chem. Eng. **39** (2008) 129.
9. *Basile, A., Paturzo, L., Gallucci, F.,* Catal. Today **82** (2003) 275.
10. *Marigliano, G., Barbieri, G., Drioli, E.,* Chem. Eng. Process. **42** (2003) 231.

11. *Brunetti, A., Caravella, A., Barbieri, G., Drioli, E.,* J. Membr. Sci. **306** (2007) 329.
12. *Brunetti, A., Barbieri, G., Drioli, E.,* Chem. Eng. Sci. **64** (2009) 3448.
13. *Piemonte, V., De Falco, M., Favetta, B., Basile, A.,* Int. J. Hydrogen Energy **35** (2010) 12609.
14. *Farsi, M., Jahanmiri, A.,* Chem. Eng. Process. **50** (2011) 1177.
15. *Rahimpour, M. R., Mirvakili, A., Paymooni, K.,* Energy **36** (2011) 1223.
16. *Ayastuy, J. L., Gutierrez-Ortiz, M. A., Gonzalez-Marcos, J. A., Aranzabal, A., Gonzalez-Velasco, J. R.,* Ind. Eng. Chem. Res. **44** (2005) 41.
17. *Levenspiel O.,* Chemical Reaction Engineering, Third Ed., John Wiley & Sons, New York, 1999.